sciendo

ARTIFICIAL SATELLITES, Vol. 57, No. SI1 – 2022
DOI: 10.2478/arsa-2022-0025

IMPROVED PREDICTION OF POLAR MOTIONS BY PIECEWISE PARAMETERIZATION

Yuanwei WU, Xin ZHAO, Xinyu YANG

Natioinal Time Service Center of Chinese Academy of Sciences, Lintong, Shaanxi, China

e-mail: yuanwei.wu@ntsc.ac.cn

ABSTRACT. On seanonal timescale, the variation of Earth rotation is mainly regulated by angular momentum exchanges between the solid Earth and the fluidal atmosphere, ocean and hydrosphere. In the 2nd EOP PCC, we developed Dill2019's method for polar motion prediction, using piecewise autoagressive parameters. The maximum prediction errors within 90 days are 36 and 16 mas for polar motion x and y components, respectively. Compared with Bulletin A, the mean absolute error of polar motion y prediction is improved by 20% in all timescale, and with a maximum improvement of 49% on the 5th day. Whereas, for polar motion x, the performance is slightly better (2% - 8%) within 30 days but worse ($-7\%\sim -19\%$) within 30$\sim$90 days. We found that the prediction accuracy is very sensitive to the quality of the angular momentum data. For example, on average, the prediction of polar motion y is around 2 times better than polar motion x. In addition, we found the accuracy of 30-90 days prediction is dramatically decreased in the year 2020. We suspect that such deterioration might be due to the pandemic of coronavirus COVID-19, which suppressed global airline activities by more than 60%, then result in a lose of air-borne meteorological data, which are important for weather forecast.

Keywords: Earth rotation prediction, Effective angular momentum functions, AAM, OAM

1. INTRODUCTION

The Earth orientation parameters (EOP) is a set of parameters that describe the direction of rotating axis of the solid Earth in both the terrestrial reference frame (TRF) and the celestial reference frame (CRF) and the rotation angle of the TRF relative to the CRF. Determination and prediction of EOP is of importance for deep space and near Earth missions, including lunar and Mars exploration, satellite navigation, positioning of celestial objects, and geophysical applications (Petit and Luzum 2010).

Variations of the polar motion (PM) and the length of day (ΔLOD/ΔUT1) can be attributted to both the external forces (tidal torques from the Sun and Moon) and internal forces that cause mass redistributions and angular momentum exchanges among the solid Earth (crust and mantle), the fluidal atmospheric, oceanic and hydrospheric components, the liquid outer core and solid inner core (Gross 2007). Once the tidal excited variations of EOP are determined and removed, the fluidal correlated features will dominate ($\sim$ 90%) in the remaining tidal free EOP series (Dobslaw et al. 2010, Dill et al. 2013).

Dill et al. (2019) demonstrated the effective angular momentum (EAM) functions, derived from numerical geophysical models of the Earth's fluidal components, are powerful data sets for the predictions of PM and ΔUT1. The EAM components χ_x, χ_y and χ_z correspond with the EOP components of PMX, PMY and ΔUT1, respectively. Using the short-term (6 days) forecast of the effective angular momentum, the mean absolute error (MAE) of PM and ΔUT1 predictions are imporved by 34.5% and 44.7%, respectively (Dill et al. 2019).

In the 2nd Earth Orientation Parameters Prediction Comparison Campaign (2nd EOP PCC), we used a method evolved from Dill2019's method; here we call piecewise parameterization which predict PM and ΔUT1 with specified parameters at different time spans. The motivation of piecewise parameterization is that there may exist better LS and AR parameters for predictions at different time stages. In Section 2, we present the technical details of the method. In Section 3, we evaluate our predictions by comparing them with both the EOP 14 C04 series and Bulletin A predictions. Summary and Conclusions are presented in Section 4.

2. PREDICTION METHODS

In Dill2019, the predictions of PM and ΔUT1 are processed in several step, as shown in Figure 1. First, the EOP series is transfered to geodetic angular momentum function (GAM) through Liouville equation. Then, the differences between GAM and EAM, are calculated and extrapolated to the next 6 days with least squares fit and autoregression (LS+AR). Third, the 6 days extrapolation of (GAM-EAM) and 6 days forcast of EAM are summed up to generate a 6-day prediction of GAM. Fourth, a 90-day GAM series is predicted with LS+AR. Finally, the 90-day prediction of PMX/PYM/UT1 is recovered from the 90-day GAM series.

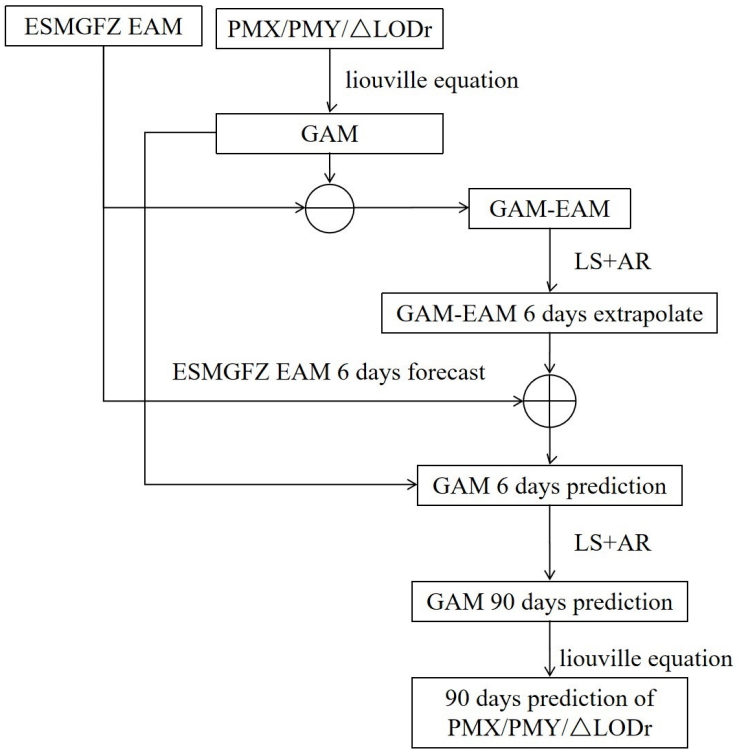

Figure 1. Flowchart for EOP prediction of Dill2019 method

Our prediction methods are evolved from Dill2019 method. In this section, we first present the discrete formulas used for GAM and EOP transformation which are not presented in Dill2019

paper. Then, the technical details of piecewise parameterization in LS and AR are presented. In this paper, we focus on the prediction method of the polar motion.

2.1 Transformation between EOP and GAM

The linearized Liouville equations that describe the relations between the EOP and GAM are presented in Equations 1 and 2

$$\frac{\Delta LOD_r}{\Lambda_0} = \chi_z(t) \tag{1}$$

where ΔLOD_r is the variation of the length of day (ΔLOD) with zonal tidal components removed and Λ_0 is the nominal length of day of 86400 seconds.

$$\vec{p}(t) + \frac{i}{\sigma_0}\frac{d\vec{p}(t)}{dt} = \vec{\chi}(t) \tag{2}$$

Given the coupling between x and y components of polar motion, the equation is written in complex notation, with $\vec{\chi}(t) = \chi_x(t) + i\ \chi_y(t)$, $\vec{p}(t) = p_x(t) - i\ p_y(t)$. Here, the negative sign in $\vec{p}(t)$ accounts for $p_y(t)$ being positive toward 90°W longitude, as the coordinates of polar motions are defined as a left-hand Cartesian coordinate system, whereas the angular momentum function components are defined in the TRF frame which is a right-hand Cartesian coordinate system.

The transformation of GAM and EOP in the z axis is straightforward; here we only give the discrete transformation formula for the x and y components for numerical use (the derivation of these two formula can be found in Barnes et al. (1983))

$$\vec{\chi}(t) = \frac{i}{2\sigma_{cw}\delta t} exp(\frac{-i\pi\delta t}{T_{cw}}) \cdot \{\vec{p}(t+\delta t) + [1 - exp(i\sigma_{cw}\delta t)]\vec{p}(t) - exp(i\sigma_{cw}\delta t)\vec{p}(t-\delta t)\} \tag{3}$$

$$\vec{p}(t) = \frac{-i\sigma_{cw}\delta t}{2} exp(\frac{i\pi\delta t}{T_{cw}}) \cdot [\vec{\chi}(t) + \vec{\chi}(t-\delta t)] + exp(i\sigma_{cw}\delta t)\vec{p}(t-\delta t) \tag{4}$$

where $\delta t = 1\ day$ is the time interval for the GAM and polar motion series, the complex Chandler frequency $\sigma_{cw} = 2\pi(1 + i/2Q)/T_{cw}$, with period $T_{CW} = 433$ days and dampling of Q = 179 (Gross et al. 2003).

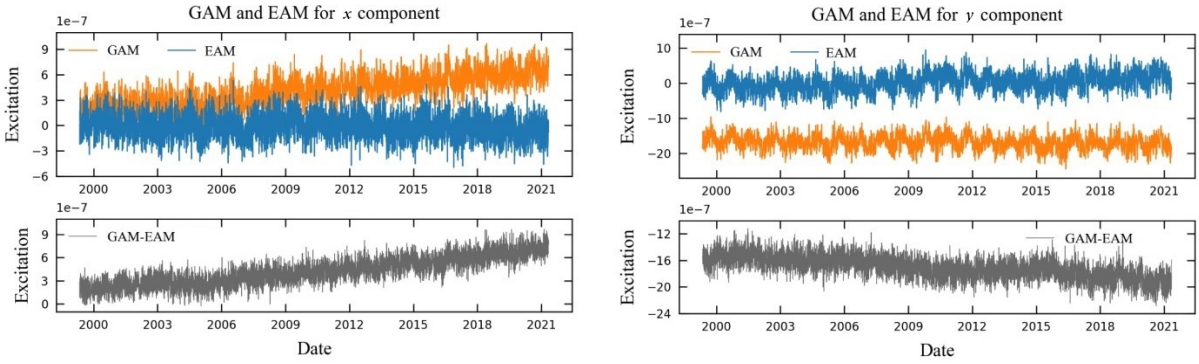

Figure 2. The transformed X (left panel) and Y (right panel) components of GAM, ESMGFZ EAM, and differences between GAM and EAM

Figure 2 shows the transformed x and y components of GAM, ESMGFZ EAM, and differences between GAM and EAM. It can be seen a remarkable correlation between GAM and EAM and seasonal oscillations in the Y component, whereas relatively lower correlation and seasonal oscillations are seen in the X component.

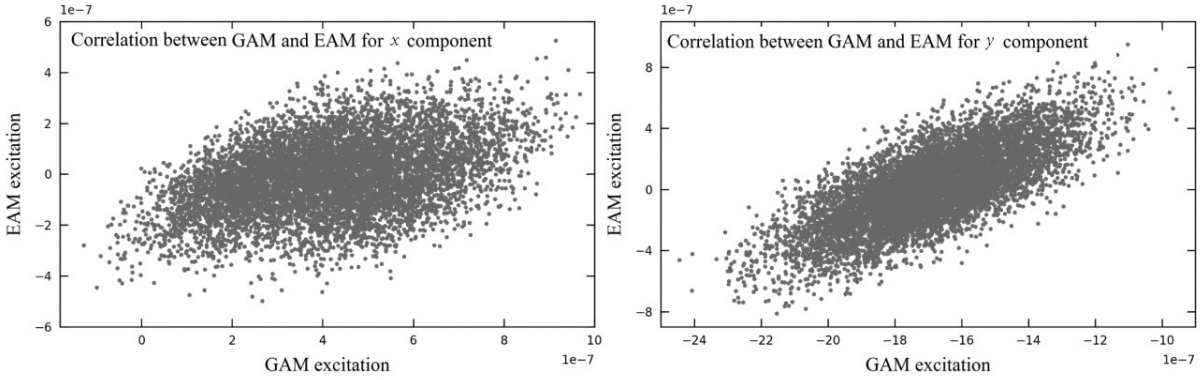

Figure 3. Correlation between GAM and EAM.
Left panel: the X component; right panel: the Y component.

In Figure 3, we present plots of GAM versus EAM to show such phenomenon. The magnitude of GAM and the correlation between GAM and EAM are higher for the Y component than that for the X component. Since the major continents of the Earth are more aligned in the Y axis that produce relatively larger excitation of PMY from atmospheric surface pressure loading, whereas atmospheric loading effect over the oceans is largely compensated by the inverted barometer response of the ocean surface (Boy et al. 2009).

2.2 Piecewise Continuous Least Squares Fit

As shown in Figure 1, there are two steps of LS+AR. The first LS+AR is used to predict the 6 days GAM-EAM series and the second LS+AR is used to predict the 90 days GAM series. The strategy of LS is same for the two steps, we fit the x and y components together in complex form,

$$\chi(t) = \begin{cases} a_1 + a_2 t \\ a_3 + a_4 t \\ a_5 + a_6 t \\ a_7 + a_8 t \end{cases} + \sum_{j=1}^{4} [b_j cos(\frac{2\pi t}{T_j} + \phi_j) + i b_j^* cos(\frac{2\pi t}{T_j} + \phi_j^*)] \tag{5}$$

where a_1, a_2, ..., a_8 are complex numbers with $a_i = (a_{real} + i a_{imag}^*)_i$, b_j and b_j^* denotes the amplitude, ϕ_j and ϕ_j^* denote the phase of the periodical componts, with $T_1 = 1\ years$, $T_2 = 1/2\ years$, $T_3 = 1/3\ years$, and $T_4 = 13.7\ days$. Same as Dill2019, the linear components are fitted every year, and the four periodic components are fitted with 4 years data. In total, we used 5 complexes, a_1, a_2, a_4, a_6, a_8, and 16 real numbers (b_j, b_j^*, ϕ_j, and ϕ_j^*) in each step of the least squares fit. a_3, a_5 and a_7 are not free parameters, because of the piecewise continuity constraint.

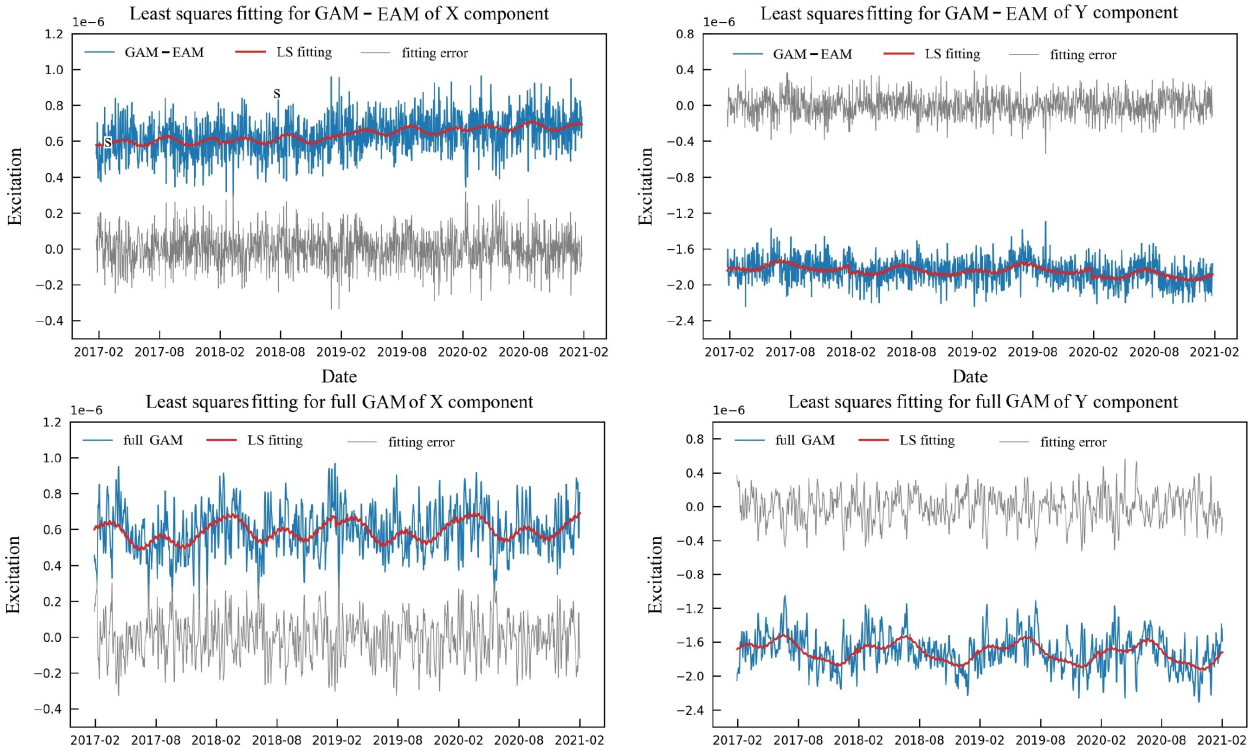

Figure 4. Piecewise continusous least squares fit of GAM-EAM (upper panels), and full GAM series (lower panels), with left panels for x component and right panels for y component. Blue lines denote data, red lines show the LS fittig results, grey lines are the LS fit residuals.

2.3 Piecewise Parameterization in AR

Up to now, the techniques we used are all identical to Dill2019. Here we present the major technical differences of our method.

For a stationary random sequence $x(t)(t = 1, 2, ..., N)$, the AR(p) model is expressed as

$$x\left(t\right) = c + \sum_{i=1}^{p} \phi_i x\left(t - i\right) + \epsilon_t. \tag{6}$$

where ϕ_i, ϕ_2, ..., ϕ_p are autoregressive coefficients, that can be solved by the Yule-Walker equations by means of the Levinson-Durbin rercursion (Brockwell and Davis 1996), and p is the order of the AR model that is determined by Akaike's Final Prediction Error (FPE) criterion (Akaike, 1971). ϵ_t is the unmodeled random noise component.

Practically, p, the order of AR model, is a critical parameter which is very sensitive to the final accuracy of prediction. In Dill2019, the p is adopted as constants, with p = 20 days for 1-6 days prediction of the equatorial components of GAM-EAM, with p = 60 days for 1-6 days prediction of the axial component of GAM-EAM, with p = 2 days for 7-90 days prediction of the equatorial component of GAM and with p = 25 days for 7-90 days prediction of the axial components of GAM.

In our prediction, we aussmed there exists a best p_n for the nth-day prediction, which is not known at the beginning but can be searched by further evaluations. Frankly speaking, such trials are still on the testing stage, and we still have no physical explanation of why some p works well than others. Therefore, feasibility of such method still needs careful evaluation. Meanwhile, in

the steps of AR, we used a modified AR formula that includes one more sampling parameter, lag,

$$\chi(t) = c + \sum_{i=1}^{p} \phi_i \chi(t-i)\, sign(i) + \epsilon_t. \tag{7}$$

with $i < p$, and $sign(i)$ is a signum function,

$$sign(i) = \begin{cases} 1 & i \,\%\, lag = 0 \\ 0 & i \,\%\, lag \neq 0 \end{cases} \tag{8}$$

The effect of the new lag parameter is a kind of desampling smooth filter . When lag equals 1, the Eq. 7 will be same as Eq. 6, whereas when lag equals 2, which means setting the odd autoregressive coefficients, ϕ_1, ϕ_3, ϕ_5, ..., in Eq. 7 as 0. Similar to the order p, the best lag is also determined by evaluation. In summary, in the process of AR, we have two parameter (p, lag), values of which are determined by evaluation.

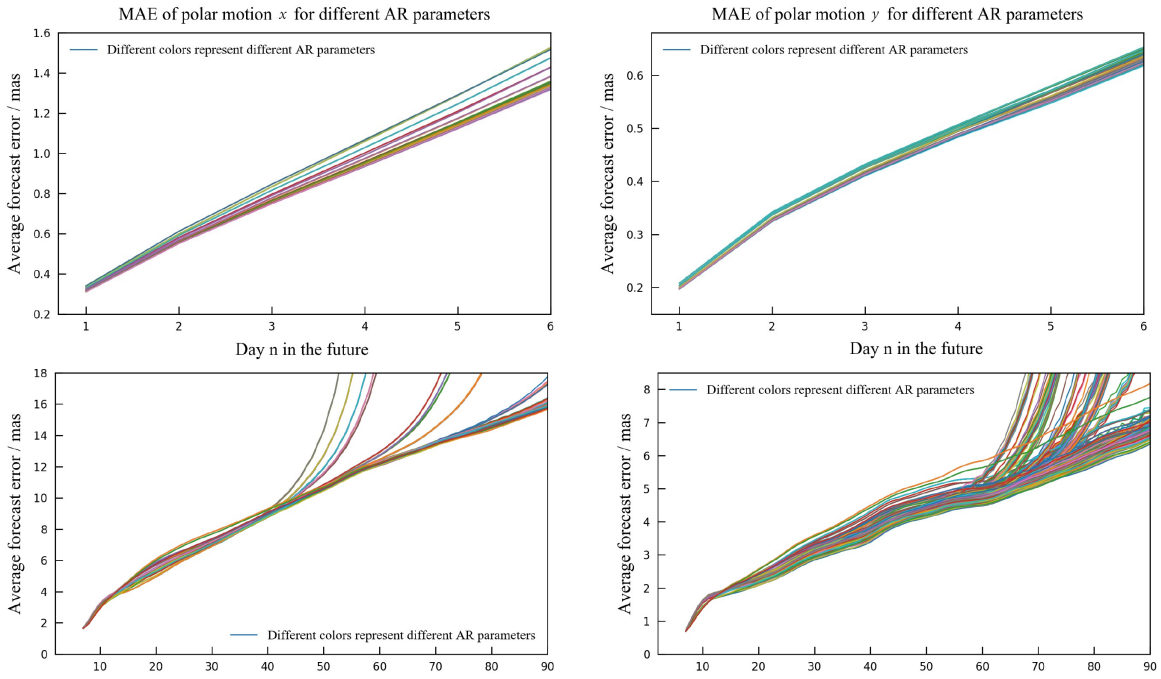

Figure 5. Mean absolute error (MAE) of prediction of polar motion x (left panels) and y (right panels) for different parameter choices for AR. Upper panels are predictions within 6 days and lower panels are predictions within 7-90 days.

Figure 5 shows exmaples of prediction for polar motions x and y, by adopting different (p, lag). It is noted that the AR is conducted for x and y components separately, whereas the LS is conducted in the complex domain for both x and y components simultaneously. It can be seen that the prediction of PMY is around 2 times better than the prediction of PMX. Given that the AR is prediction of noisy signals, and χ_x are much more noisy than χ_y, a better prediciton of PMY than PMX is explicable. Especially, within 6 days, the selection of (p, lag) is very sensitive for prediction of PMX.

Asumming there exists best (p, lag) of AR, we make a large amount of trials and prediction of EOPs in 441 days from Sep. 2019 to Feb. 2021 to find the best AR parameter (p, lag). For the

prediction of GAM-EAM within 6 days, we searched p within the range of [10,90] and searched the lag within the range of [1, 20]. For AR of GAM within 7 to 90 days, we searched p within the range of [2, 20], and lag within the range of [1,20]. In Tables 1 and 2, given are the best AR parameters (p, lag) we adopted for the polar motion x and y, respectively.

Table 1. Best autoregressive parameters for prediction of PMX

Future day	p **for PMX**	p **for PMY**	lag **for PMX**	lag **for PMY**
1-2	60	60	5	15
3-6	60	60	1	15
7-10	18	18	16	16
11-13, 37-38, 41-42	8	8	2	2
14	5	3	1	1
15-20, 24, 28-29	2	3	1	1
21-23, 25-27, 30	4	4	2	2
31-34	5	19	1	1
35-36,39-40	6	6	2	2
43-57, 65-75	8	8	3	3
58, 62-64	20	20	18	18
59-61	19	19	17	17
75-90	10	10	6	6

Table 2. Best autoregressive parameters for prediction of PMY

Future day	p **for PMX**	p **for PMY**	lag **for PMX**	lag **for PMY**
1-6	19	19	1	1
7	19	19	17	17
8-11	20	20	18	18
12	6	6	2	2
13-14,16-67,73-90	4	4	2	2
15	3	2	1	1
68-72	8	8	2	2

3. EVALUATIONS

3.1 Comparison with IERS EOP C04

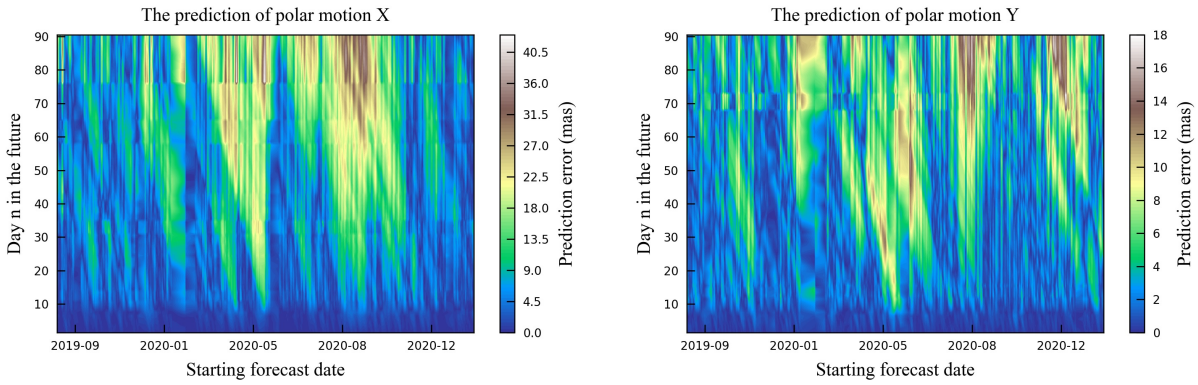

Figure 6. Absolute difference between polar motions series of IERS EOP C04 and our predition up to 90 days

In Figure 6, shown are the prediction errors for all the 441 predictions from Sep. 2019 to Feb. 2021. Within 90 days, the maximum prediction error of PMX is 36 mas, the maximum prediction error of PMX is 16 mas; within 10 days, the maximum prediction errors of PMX and PMY are 4.5 and 2 mas. On an average, the prediction of PMY is around 2 times better than that of PMX. In addition, we found that the prediciton errors of PMX are much higher in 2020 than 2019. In 2019 September, the prediction errors of both PMX and PMY are lower than 10 mas, whereas in 2020 August and September, the 30-90 days prediction errors are around 2 or even 3 times higher than that of 2019. We suspect that such phenomenon might be due to the pandemic of coronavirus COVID-19, which result in a decrease in global airline by more than 60%. As the air-borne meteorological radar data are very important for numerical weather model, a decrease of flight number finally results in worse weather and AAM forecast, and then worse EOP prediction. A future study on evaluation of whether and/or how much the AAM data might be influenced by the lack of air-borne meteorological data can be helpful to verify or deny such hypothesis.

3.2 Comparison with IERS bulletin A prediction

To compare with IERS bulletin A prediction, in Figure 7, we show the MAE of both our prediction and IERS bulletin A prediction. Our prediction of PMY is better ($\sim$20%) than bulletin A prediction in all timescale. Especially, on the 5th day and 90th day, the MAE is reduced by 49.0% and 28.9%, respectively. For the prediciton of PMX, within 30 days, our predictions are slightly better (2% - 8%) than bulletin A, but become worse ($-7\%\sim -19\%$) than bulletin A within 30-90 days. In Table 3, we present the prediction errors (MAE) at different future days.

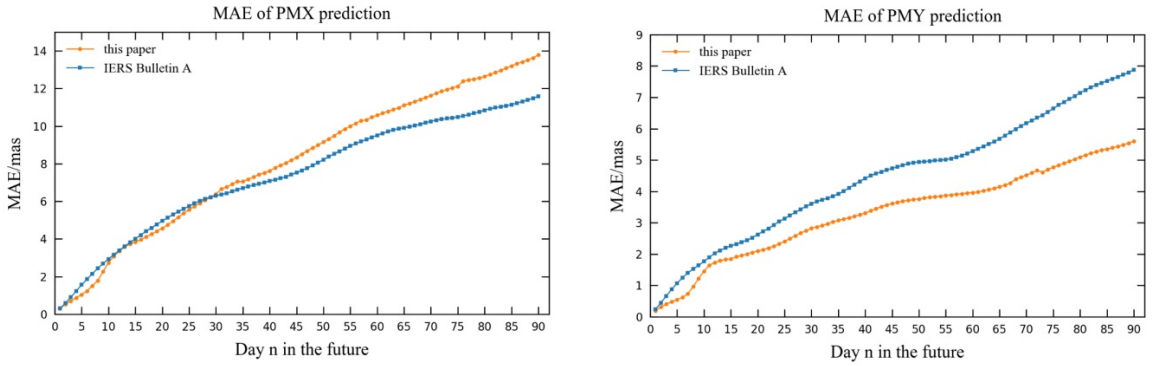

Figure 7. Comparing the MAE of our 90-day prediction with the MAE of IERS bulletin A 90-day prediction

Table 3. PM prediction errors (MAE) at different future days

	1 days	**5 days**	**10 days**	**20 days**	**40 days**	**60 days**	**90 days**
PMX forecast of this paper (milli arcsec)	0.30	1.04	2.74	4.57	7.62	10.58	13.78
PMX forecast of IERS (milli arcsec)	0.31	1.56	2.93	4.95	7.08	9.51	11.57
PMX forecast error reduction (%)	2.62	32.98	6.59	7.74	−7.67	−11.23	−19.07
PMY forecast of this paper (milli arcsec)	0.19	0.54	1.46	2.10	3.31	3.97	5.60
PMY forecast of IERS (milli arcsec)	0.24	1.07	1.76	2.62	4.42	5.28	7.89
PMY forecast error Reduction (%)	20.77	48.98	17.53	20.05	25.13	24.97	28.93

4. CONCLUSIONS

In the 2nd EOP PCC, we developed Dill2019 method for prediciton of polar motion by adopting different autoagressive parameters at different prediction stages. In steps of AR extrapolation, we introduced a lag parameter, aiming to reduce random errors by desampling the LS residuals. The best parameters we adopted are determined by trials and evaluation. Our method works well for the polar motion y component, with a maximum prediction error of 16 and an MAE of 12 in 90 days. However, the prediction of PMX is around 2 times worse than PMY. We still need further evaluations to verify both the feasibility of the method and the applicability of the "optimized" parameters currently used. We found that the prediction accuracy is highly correlated with the quality of the AAM data. For exmaple, the prediction accuracy of PMY is around 2 times better than PMX. Additionally, we found that the 30-90 days prediction accuracy in 2020 is around 2 times worse than that in 2019. We suspect that this might be due to the decline of the air-borne meteorological data in 2020 caused by the pandemic of coronavirus COVID-19.

Acknowledgments. This publication makes use of EOP data from the International Earth Rotation and Reference Systems Service (IERS) and of AAM, OAM, HAM, SLAM data from the Earth System Modelling group at Deutsches GeoForschungsZentrum, ESMGFZ. We appreciate Doctor Dill R's kind guidance on how to use the ESMGFZ data.

REFERENCES

Akaile, H., (1971) Autoregressive model fitting for control, *Ann. Inst. Stat. Math.*, Vol. 23, 163-180.

Barnes R.T.H., Hide, R., White A.A. Wilson, C.A., (1983) Atmospheric angular momentum fluctuations, length-of-day changes and polar motion, *Proc. R. Soc. Lond. A*, Vol. 387, 31

Boy J.P., Longuevergne L., Boudin F., Jacob T., Lyard F., Llubes M., Florsch N., Esnoult M.F., (2009) Modelling atmospheric and induced non-tidal oceanic loading contributions to surface gravity and tilt measurements, *Journal of Geodynamics*, Vol. 48, Issues 3–5, 182-188

Brockwell, P.J., Davis, R.A., (1996) Introduction to Time Series and Forecasting, *Springer*, New York, 420 pp.

Dill R., Dobslaw H, Thomas M. (2013) Combination of modeled shortterm angular momentum function forecasts from atmosphere, ocean, and hydrology with 90-day EOP predictions, *Journal of Geodesy*, Vol.87, 567–577

Dill R., Dobslaw H, Thomas M. (2019) Improved 90-day Earth orientation predictions from angular momentum forecasts of atmosphere, ocean, and terrestrial hydrosphere, *Journal of Geodesy*, Vol.93, 287–295

Dobslaw H., Dill R., Grötzsch A., Brzezinski A., Thomas M. (2010) Seasonal polar motion excitation from numerical models of atmosphere, ocean, and continental hydrosphere. *Journal of Geophysical Research (Solid Earth)*, Vol. 115, Issue B10, 406-417

Gross R.S., Fukumori I., Menemenlis D. (2003) Atmospheric and oceanic excitation of the Earth's wobbles during 1980-2000. *Journal of Geophysical Research*, Vol. 108, 2370

Gross R.S., (2007) Earth Rotation Variations - long period, *Phisical Geodesy*, eds. Herring T. A., Treatise on Geophysics, Vol. 11, Amsterdam, 2007

Petit G. & Luzum B. (2010) *IERS Technical Note 36*, IERS Conventions (2010)

Received: *2022-07-01*

Reviewed: *2022-09-17 (undisclosed name); 2022-09-24 (undisclosed name)*

Accepted: *2022-12-09*